Understanding the chemical pathways of NO formation in low-pressure burner stabilized premixed lean-to-rich hydrogen flames

Tirthankar Mitra, Nathalie Lamoureux, Pascale Desgroux

Combustion and Flame 277 (2025) 114192

Contents lists available at ScienceDirect

Combustion and Flame

journal homepage: www.sciencedirect.com/journal/combustion-and-flame

Understanding the chemical pathways of NO formation in low-pressure burner stabilized premixed lean-to-rich hydrogen flames☆

Tirthankar Mitra *, Nathalie Lamoureux, Pascale Desgroux *

CNRS, UMR 8522, PC2A-Physicochimie des Processus de Combustion et de l'Atmosphère, Université de Lille, Lille F-59000, France

ARTICLE INFO

Keywords:
Hydrogen combustion
Laser diagnostics
NO_X
NNH
Chemical modelling

ABSTRACT

Hydrogen (H_2) combustion, a potential clean energy solution, is hindered by NO emission that affects human health and the environment. A comprehensive understanding of NO formation during H_2 combustion is necessary to mitigate its emission. The dynamic interplay between the different formation pathways makes the interpretation of NO sub-mechanism difficult. Lack of comprehensive experimental data further limits the comprehension of NO formation process, especially for the non-thermal NO formation pathways. In this study, quantitative NO and temperature measurements were performed using in-situ laser diagnostics in 6 low-pressure burner stabilized $H_2/O_2/N_2$ flames over a wide range of equivalence ratios (0.35–1.50) at 35 and 70 Torr (4.67, and 9.33 kPa). The maximal temperature in the flames remain below 1500 K, which minimizes the thermal NO pathway and allows for a focused study of non-thermal pathways of NO formation. However, the low temperature restricts NO formation imposing severe challenges on experimental measurements. Several precautions were taken to address these challenges and reduce the experimental uncertainty. The maximal NO mole fraction in the flames is between 0.09 and 0.71 ppm. The experimental re-evaluation of two flames similar to Harrington (Harrington et al., Proc. Combust. Inst., 26, 1996) shows disagreement with the original experimental data but consistent with the simulation predictions. This re-evaluated dataset can potentially replace the existing controversial Harrington measurements for validation of NNH pathway. The simulations of the flames using three recent chemical kinetic models predict NO in satisfactory agreement with the experiment, even for the flames similar to Harrington. The study suggests that NNH pathway dominates NO formation in low-pressure, low temperature H_2 combustion irrespective of the equivalence ratio. The large set of novel experimental datasets generated in this study can serve as future chemical kinetic model validation targets, especially for the NNH pathway of NO formation.

1. Introduction

The intense race towards net-zero emissions has led to the development of several alternative energy technologies. Hydrogen (H_2) combustion, in particular, has emerged as a potential solution for decarbonizing several industrial sectors, especially hard-to-abate sectors like cement, chemicals, iron, and steel. However, H_2 combustion emits NO, precursors of photochemical smog and acid rain [1]. Therefore, it is imperative to understand the NO formation pathways to develop suitable emission mitigation strategies for H_2 combustion.

There is a consensus that there are three pathways of NO formation during H_2 combustion: thermal, N_2O, and NNH [1]. Fig. 1 shows the simplified schematic of the different pathways. Among these pathways, the thermal pathway, popularly known as the Zeldovich pathway [2], can be avoided by maintaining a combustion temperature well below 1700 K. NO formation through the N_2O pathway begins by the direct recombination of N_2 and O in the presence of a third body forming N_2O [3,4]. The third body decreases the activation energy of the recombination step, making it favorable at lower temperatures and higher pressure [5]. N_2O can lead to NO formation by reacting with H or O [1]. However, NO formation from N_2O competes with N_2 recycling from N_2O [1,6]. The formation of NO via the NNH pathway involves the formation of NNH via the reaction $N_2+H \rightleftharpoons NNH$, followed by oxidation of NNH [7]. The NNH oxidation step competes with the recycling of NNH to N_2 [8]. In addition, the oxidation of NNH can lead to the formation of N_2O, cross-linking the two NO formation pathways [1]. The N_2O pathway is

* Corresponding authors.
E-mail address: pascale.desgroux@univ-lille.fr (P. Desgroux).

https://doi.org/10.1016/j.combustflame.2025.114192
Received 4 December 2024; Received in revised form 15 April 2025; Accepted 15 April 2025
Available online 24 April 2025

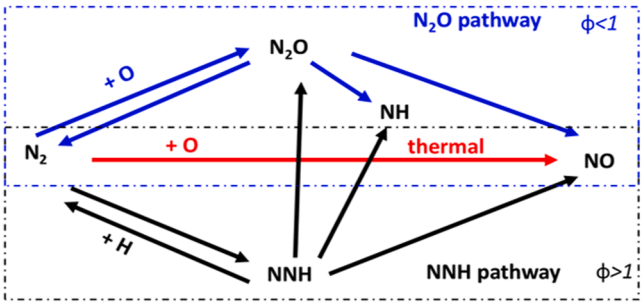

Fig. 1. A simplified schematic showing different pathways for NO formation in H_2 combustion.

relevant under lean conditions at high pressures and moderate temperatures, while the NNH pathway is important at short residence times and all temperatures [9,10]. The formation of NO during combustion can occur concurrently with NO consumption/reduction. Under reducing conditions, NO is recycled to N_2 via NH intermediate [9]. The above discussion manifests the complexities and interdependencies between the different steps involved in the NO formation process.

Several chemical kinetic models have been developed to decouple the concerted chemical pathways, breaking the global pathway into crucial elementary reactions for a detailed comprehension of the NO formation process. The models rely on experimental NO data to assess their performance and identify the scope for improvements, especially for the NNH pathway, since no experimental rate coefficient is available for the NNH sub-mechanism. Most of the NO measurements have been performed in the combustion of H_2 doped with $NO/N_2O/NH_3$ [11–26]. These experimental studies provide valuable insights into the oxidation/reduction of N-containing intermediates, but they cannot shed any light on how the NO formation begins in combustion systems that only contain N_2 and no N-containing intermediates. Thus, NO measurements in neat H_2 combustion are necessary to understand NO formation pathways comprehensively.

Only a limited number of experimental studies exist for neat H_2 combustion. These studies can be divided into ex-situ and in-situ studies. The pioneering study of Homer and Sutton [27] measured the NO mole fractions in premixed atmospheric pressure $H_2/O_2/N_2$ flames with an equivalence ratio (ϕ) ranging from 0.7–1.1 using the Saltzman technique. Most ex-situ studies utilize NO_x chemiluminescence analyzers for measuring NO [28–31]. Xie et al. [28] measured the NO mole fractions in atmospheric lean ($\phi = 0.6$–0.7) H_2/air mixtures in a jet-stirred reactor with a residence time of 5.3 to 35 ms. The results show that the NO formation below 1700 K is independent of residence time and moderately dependent on temperature, suggesting the presence of non-thermal NO formation pathways. Hayhurst and Hutchinson [29] performed NO measurements in atmospheric $H_2/O_2/N_2$ flames at $\phi = 1.5$ with peak temperatures of 2290 and 1840 K. The consequent analysis of the experimental data shows that in flame with a peak temperature of 1840 K, the NNH pathway contributes 3 times more to NO formation than the thermal pathway, while in the flame with a peak temperature of 2290 K, the contribution from both the pathways are equal. Rørtveit et al. [30] measured the NO mole fractions in nine counterflow diffusion flames of H_2 having peak temperatures in the range 1835–2125 K. The comparison between experimental data and numerical simulation revealed that N_2O and NNH pathways dominate at lower temperatures. Purohit et al. [31] measured NO_x emission in atmospheric jet-stirred reactor combustion of H_2/air system over a range of ϕ (0.8–1.3) with temperatures in the range 1635–1525 K. The experimental data shows that the N_2O pathway is dominant in the lean condition, while the NNH pathway is dominant in the rich condition.

The in-situ studies of NO formation mainly utilize Laser Induced Fluorescence (LIF) technique [32–35]. Harrington et al. [32] measured the NO profiles in low-pressure (5.07 kPa and 10.39 kPa) rich ($\phi = 1.5$) H_2/air flames (peak temperature = 1200 K), which promote the NNH pathway. The NO measurements of Harrington et al. are experimental evidence of the NNH pathway, confirming the prediction of [7]. Durocher et al. [33] studied the NO formation in jet-wall stagnation atmospheric H_2/air flames with $\phi = 0.7$–1.5 and peak temperatures in the 1725–1785 K range. The subsequent analysis of the experimental data shows that in the lean flame, NO is primarily formed through the NNH pathway with minor contributions from the thermal pathway, while in the rich flame, the NNH pathway is the sole source of NO formation. The NO concentration measurements in high pressure (2 - 8 atm.) near stochiometric (ϕ =0.975) H_2/Air/He flames (peak temperatures: 1530–1800 K) highlight that the NNH pathway is the primary source of NO formation even at high pressure [34]. Meulemans et al. [35] measured the NO mole fractions in atmospheric pressure stochiometric premixed H_2/Air/Ar flames with peak temperatures in the 1600–2300 K range. The measurements show significant discrepancies with the numerical simulation, mainly due to inaccurate prediction of radical pool driving the NO formation [35].

In summary, the process of NO formation in H_2 combustion is convoluted and needs the help of chemical models to unravel the underlying pathways. The experimental data in the literature are limited to only a handful and a few combustion conditions. The scarcity of experimental data limits the fundamental understanding of the NO formation process in H_2 combustion. Glarborg et al. [1] remarked that the NNH pathway remains controversial in the literature. Durocher et al. [33] found that tuning the reaction rates to generate a nominal mechanism that matches the validation targets can contain discrepancies at the basic chemistry level. The interpretation of the numerical predictions in terms of NO formation sub-mechanisms is ambiguous in the literature [36], which further hinders the comprehension of NO formation. A detailed understanding of NO formation is paramount in turbulent H_2 combustions, which are essential for practical applications. Turbulent premixed H_2 combustion creates non-uniform chemical and thermal environments where the different pathways of NO formation (including non-thermal pathways) can play a dynamic role in NO formation [37,38]. In order to unravel the chemical pathways of NO formation in turbulent H_2 combustion, it is necessary to have a better understanding of the different pathways of NO formation during H_2 combustion.

To improve our understanding of NO formation, experimental datasets for combustion conditions that restrict NO formation to small chemical subsets at a time are desirable. The current study has studied six laminar low-pressure $H_2/O_2/N_2$ flames with $\varphi = 0.35$–1.50. Laminar premixed flames facilitate the investigation of chemical pathways by varying the chemical environment (ϕ) without any complicated fluid dynamics. The peak temperatures in the flames are maintained in the range of 1200–1500 K to suppress thermal NO, as confirmed by supplementary numerical simulations. Quantitative NO measurements have been made along the vertical axis of the flames using the LIF technique, followed by calibration of the obtained signals. The flames have also been simulated using three recent chemical kinetic models available in the literature with the updated hydrogen and NO_X sub-chemistry. As mentioned earlier, the different pathways of NO formation are interconnected, making it difficult to quantify the contributions of different pathways existing in the flames. Thus, in the current study, instead of quantifying the contributions of different NO pathways, integrated flux analyses of species are performed to determine how N_2 is converted into NO through different intermediates. The novelty of the study lies in the fact that it provides an original experimental NO dataset under a wide range of fuel conditions. The flame conditions of Harrington et al. [32] have been revisited in this study. The re-evaluated dataset shows the potential to resolve the discrepancy between the experiment and the model related to the NNH pathway that has existed for over 3 decades.

2. Experimental methods

2.1. Burner configuration and flame conditions

A 6-cm diameter bronze water-cooled (298 K) McKenna burner (Holthuis & Associates) is used to stabilize $H_2/O_2/N_2$ premixed flames. The burner is placed in a stainless-steel pressure enclosure. The pressure inside the enclosure is maintained using an automatic pressure regulator (Leybold C MOVE) and a rotatory vacuum pump (Leybold SOGEVAC SV 25 D). The exhaust steam is trapped using a chiller cooled to 274 K. The burner enclosure has several optical ports allowing in-situ laser diagnostics (LIF). The burner can move vertically. All the measurements were performed along the vertical axis of the burner. The Height Above Burner (HAB) is measured using a digital caliper with an accuracy of 10 μm.

The volumetric flow rate of the inlet gases is maintained by mass flow controllers (Bronkhorst EL-FLOW Prestige for H_2, Tylan FC-260 for O_2 and N_2). The reported accuracy for the H_2 mass flow controller is 0.5 % of the reading value + 0.1 % of the full scale, and that for the others is 1 % of the full scale. To ensure high repeatability in the volumetric flow rate, the power supply and controller of the mass flow controllers have 3 digits of accuracy. The purity of O_2, N_2, and H_2 are 99.995 %, 99.99 %, and 99.999 % respectively.

Five flames at 4.67 kPa (35 Torr) with ϕ ranging from 0.35 to 1.50 were studied. The flame with $\phi = 1.50$ was also studied at 9.33 kPa (70 Torr). Table 1 reports the flame conditions for all the flames. The fuel mixture composition was chosen so that the peak temperature in the flames remains well below 1500 K. The total volumetric flow rate was maintained at 4.6 slpm approximately for all the flame conditions. The $O_2/(O_2+N_2)$ ratio was maintained close to 0.26. This dilution ratio ensured flame stability. For the richest flame, it was possible to decrease the ratio down to 0.21 bringing the current flame conditions as close as possible to those of Harrington et al. [32].

2.2. Laser diagnostics setup

The relative NO concentrations were measured using the LIF technique. Fig. 2 shows a schematic of the laser diagnostic setup. A tunable dye laser (Quantel TDL90+) pumped by a ns pulsed frequency-doubled Nd:YAG laser (Quantel Q-smart 850) was used to excite the NO molecules. The fundamental dye radiation ($\lambda \approx 572$ nm) is doubled and mixed with the Nd:YAG residual radiation at 1064 nm, generating output wavelengths of around 226 nm. NO profiles were measured in the linear regime ($E \leq 0.7$ mJ/cm^2 per pulse) of the LIF excitation using the mixture of $Q_1(16.5)$ and $Q_{21}(16.5)$ transitions of the $A^2\Sigma^+ - X^2\Pi(0,0)$ band of NO at 225.95 nm. Hereafter, this transition will be mentioned as $Q_1(16.5)$. The spectral laser bandwidth at 226 nm was estimated to be around 0.7 cm^{-1} [39]. The rotational level J" = 16.5 was chosen for excitation because it has the highest ground state population at 1400–1500 K, the expected maximum flame temperature. Additionally, the Boltzmann fraction for J" = 16.5 varies by only 14 % over the 300–1500 K temperature range. To minimize the problems of scattering for HABs close to 0, the laser beam was cut into (y × z) = 4 mm × 0.4 mm with the help of a pinhole and a horizontal rectangular slit. The laser beam was introduced into the pressure enclosure parallel to the burner surface and perpendicular to the burner axis. A photodiode after the burner records the energy fluctuations of the incident laser beam.

Table 1
Equivalence ratio (ϕ), mole fractions of H_2, O_2, and N_2, total flow rate, and pressure for all the flames studied. The total flow rate is in slpm (at 273.15 K and atmospheric pressure, 101.3 kPa).

ϕ	χ_{H2}	χ_{O2}	χ_{N2}	Total flow rate (slpm)	$O_2/(O_2+N_2)$	Pressure kPa (Torr)
0.35	0.152	0.221	0.627	4.625	0.260	4.667 (35)
0.60	0.239	0.197	0.564	4.610	0.259	4.667 (35)
1.05	0.352	0.170	0.479	4.590	0.259	4.667 (35)
1.30	0.404	0.155	0.440	4.450	0.260	4.667 (35)
1.50	0.387	0.129	0.484	4.650	0.210	4.667 (35)
1.50	0.387	0.129	0.484	4.650	0.210	9.333 (70)

The LIF signal was collected through $f = 200$ mm lens and focused on the entrance slit of a spectrometer using $f = 350$ mm lens (total magnification = 1.5). The vertical resolution (z) of the LIF measurements was restricted to 0.4 mm, imposed by the width (z = 0.6 mm) of the entry slit of the spectrometer. The final probing volume was 0.4 mm (z) × 10 mm (x) × 4 mm (y). The spectrometer (SP2500i, f/6.5, Acton Research) has a 1200 gr/mm grating blazed at 300 nm. The signal intensity collected along the $A^2\Sigma^+ - X^2\Pi(0,2)$ band of NO was extremely low in the lean and the rich flames. Hence, the output slit was adjusted to obtain a collection bandwidth of 20 nm, centered at 240 nm for collecting both (0,1) and (0,2) bands of NO. The signal was collected using a photomultiplier tube (XP2020Q, 1.5 ns rise-time, Photonis) and sampled using a digital oscilloscope (HDO4000, 12-bit vertical resolution, 1 GHz bandwidth, 1.25 GS/s, LeCroy). Signals were treated in real-time using a Labview program. Further details on the acquisition and processing of very weak LIF signals, due to the very low NO mole fraction, are given in Section S1 in the Supplementary Information.

2.3. NO LIF profiles

Measurements of LIF profiles in the investigated flames were challenging due to the low density of NO formed in the low-pressure flames, especially in the $\phi = 1.50$ flames. Fig. 3 compares the intensity of the NO $Q_1(16.5)$ peak in $\phi = 1.05$ flame doped with 10 ppm of NO (black dots) and in undoped $\phi = 1.05$ flame (red dots) at HAB = 3.0 cm. The spectra were recorded at 0.5 pm/s scan speed (in the fundamental wavelength) and averaged over 10 laser shots. The signal in the undoped flame is more than 1 order of magnitude less than in the doped flame. The signals decrease more for the lean and rich flames. One of the biggest challenges imposed by low signal intensity was tuning the laser wavelength to be precisely at the peak of the transition. To address this challenge, the laser wavelength was precisely tuned in the burnt gas region of the undoped $\phi = 1.05$ flame with maximum laser energy (typically 1.4 mJ/cm^2 per pulse). Once tuned, the laser was stable for at least 1 hour, allowing for complete LIF profile measurements along the HAB for a single flame. For the NO LIF profiles, the laser energy was decreased to 0.7 mJ/cm^2 per pulse after wavelength tuning. The tuning was performed before each set of measurements.

The NO LIF profiles in each flame were constructed by measuring the temporal peak of the LIF signals (prompt-LIF) (insert of Fig. 2). In low-pressure flames, the LIF temporal decay (19 ns) is longer than the laser pulse duration (5 ns), which eliminates the need for quenching correction as verified in [40]. The prompt-LIF signals were averaged over 1000 laser shots to improve the S/N ratio. Signals were also recorded at wavelength away from the excitation peaks (off-resonance) for all the measurements and subtracted from the prompt-LIF signals to correct for noise and interferences (see supplementary information S1). For each flame condition, the NO LIF profiles were recorded multiple times (at least 3). The precision in the LIF profiles is 5 % approximately. Each LIF profile was normalized against the signal recorded at HAB = 3.0 cm. The normalized LIF profiles for each flame condition were averaged to obtain an average normalized LIF profile.

2.4. Temperature measurements

The temperature was measured using the multi-line NO LIF thermometry by scanning the laser wavelength from 225.45 to 225.72 nm, as recommended in [39]. For the temperature measurements, the N_2 in the fuel mixture was substituted with 50 ppm of NO using a commercial 2 % NO in N_2 cylinder. The exit slit of the spectrometer was reduced to have a bandwidth of 10 nm with a center of 246 nm allowing the collection of the entire A-X (0,2) vibrational band of NO. The entrance

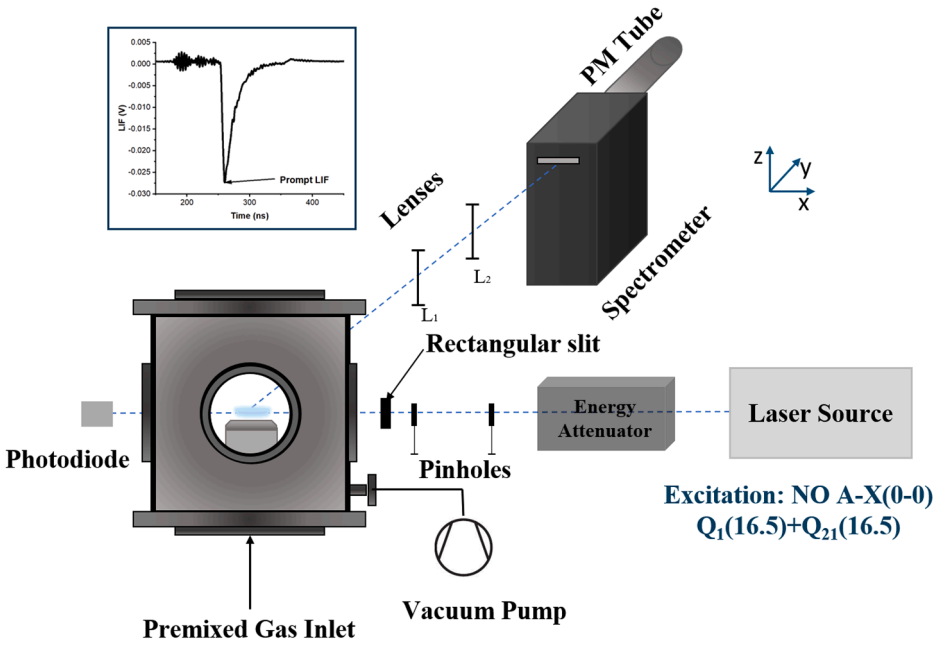

Fig. 2. Schematic of laser diagnostic setup. Insert shows the temporal prompt LIF signal.

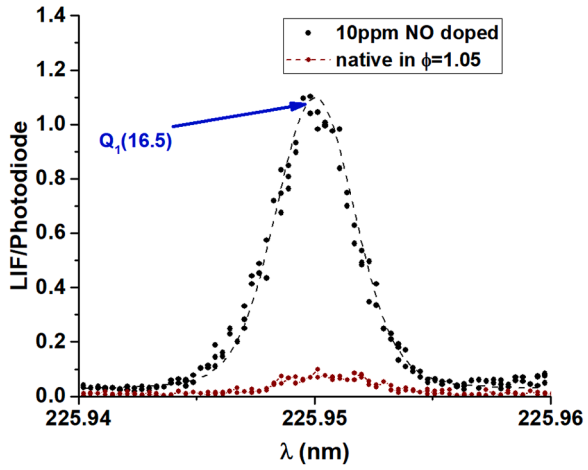

Fig. 3. Comparison of $Q_1(16.5)$ peak intensity in $\phi = 1.05$ flame doped with 10 ppm NO (black dots) and undoped $\phi = 1.05$ flame (red dots) at HAB = 3.0 cm.

slit of the spectrometer was reduced, resulting in an effective probing volume of 0.3 mm (z) × 10 mm (x) × 4 mm (y). Measurements were performed in the linear regime of LIF. Temperature is derived by fitting the experimental spectrum to the theoretical one using the Thermo-NO-LIF software [39,41]. The Thermo NO-LIF software automates the fitting process (including Voigt broadening) providing a consistent approach to evaluate NO-LIF spectra and derive temperature. The accuracy and repeatability of multi-line NO LIF thermometry is 4 % [39]. Due to scattering effects, temperatures cannot be measured below HAB = 0.06 cm.

2.5. Absolute quantification of normalized NO LIF profiles

The relation between the LIF signal and the mole fraction can be described by Eq. 1.

$$\chi_{NO} \propto \frac{S_{LIF}}{PHD} \times \frac{1}{f_B(J'', T)} \times T \times \frac{1}{p} \tag{1}$$

where χ_{NO} is the NO mole fraction, S_{LIF} is the LIF signal (V), PHD is the photodiode signal (V) captured after the burner, f_B is the Boltzmann fraction for $J'' = 16.5$ at temperature T, and p is the pressure. The conversion of average normalized LIF profiles into mole fraction profiles involved 3 steps. First, a separate experiment was conducted to compare the LIF signals in all the flames at HAB = 3.0 cm against that in $\varphi = 1.05$ flame at the same HAB, yielding the LIF switch ratio (L.S.) for each flame condition. By scaling the individual average normalized LIF profiles with the corresponding L.S., the LIF profiles for all the flame conditions were related to each other, yielding in the relative NO LIF profiles.

Second, the HAB = 3.0 cm in the flame $\varphi = 1.05$ was chosen as the reference point and the native NO mole fraction at the reference point was determined using the standard addition method [42,43]. N_2 in the inlet fuel mixture was substituted (total volumetric flow rate was kept constant) with diluted NO to achieve NO doping ranging from 0 to 8 ppm at HAB = 3.0 cm. A commercial 2000 ppm NO in N_2 cylinder (99.95 % purity) was used for NO doping. The volumetric flow rate of diluted NO was controlled using a separate mass flow controller (Bronkhorst F201 CV, 30sccm) with a reported accuracy of 0.5 % of the full scale. The nitrogen supply was divided into two parts for precise calibration: a constant higher flow rate using a 5-slpm mass flow controller and an auxiliary flow controlled using a 100-sccm mass flow controller (low-ΔP-flow F-201 DV, Bronkhorst). The auxiliary flow was manipulated to compensate for the diluted NO injected through the 30 sccm mass flow controller. The on and off-resonance LIF signals were recorded for every NO doping level (m). A dimensionless variable Y_m was calculated using Eq. 2.

$$Y_m = \frac{\left(\frac{S_{LIF}}{PHDON}\right)_m - \left(\frac{S_{LIF}}{PHDOFF}\right)_m}{\left(\frac{S_{LIF}}{PHDON}\right)_{native} - \left(\frac{S_{LIF}}{PHDOFF}\right)_{native}} - 1 \tag{2}$$

The values of Y_m were plotted against m, and fitted using a linear fit. The native NO mole fraction at the reference point was derived from the inverse of the slope of the linear fit. Three sets of calibrations were performed. Fig. 4 shows the calibration curves for all the three sets. The average native mole fraction in the $\phi = 1.05$ flame at HAB = 3.0 cm is 0.71 ppm with a standard deviation of 5 %.

The standard addition method was also applied in the $\phi = 0.35$ flame at HAB = 3.0 cm. The value of the native mole fraction of NO (0.18 ppm)

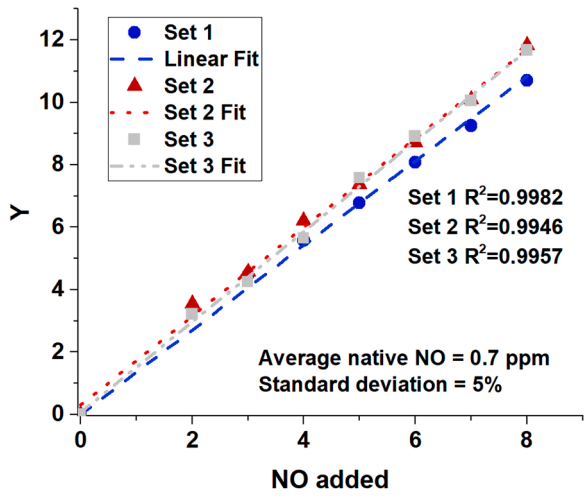

Fig. 4. Calibration curves obtained from the 3 calibration sets.

is in perfect agreement with that resulting from the LS applied between the stoichiometric (calibrated) and the lean flames, confirming the robustness of the calibration method.

Finally, the relative NO LIF profiles were converted into mole fraction profiles by using Eq. 1 along with the temperature and the derived native NO mole fraction at the reference point.

2.6. Calculation of uncertainty in mole fraction measurements

The final mole fraction derived from the LIF technique is a function of S_{LIF}, PHD, L.$S.$, T, and the native mole fraction derived for the reference point (Cal). The total uncertainty in the mole fraction is calculated by applying Taylor series expansion resulting in Eq. 3:

$$\frac{\delta\chi}{\chi} = \left(\left(\frac{1}{\frac{S_{LIF}}{PHD}} \times \delta\left(\frac{S_{LIF}}{PHD}\right) \right)^2 + \left(\frac{\delta(L.S.)}{L.S.}\right)^2 + \left(\frac{\delta(T)}{T}\right)^2 + \left(\frac{\delta(Cal)}{Cal}\right)^2 \right)^{0.5} \tag{3}$$

where $\delta\left(\frac{S_{LIF}}{PHD}\right)$ is the standard deviation in the LIF signal, $\delta(L.S.)$ is the standard deviation in the L.S. ratio, $\delta(T)$ is the standard deviation in temperature and $\delta(Cal)$ is the standard deviation in calibration. The maximum standard deviation for these parameters is 6 %, 7 %, 6 %, and 5 %, respectively. Using these values, the resulting maximum total uncertainty in the mole fraction profile is 13 %. This value has been used to determine the uncertainty in all the mole fractions discussed in this study.

3. Numerical simulation

3.1. Kinetic modeling

The kinetic modeling was performed using the Ansys-Chemkin PREMIX code [44]. The volumetric flow rate and the mole fraction of the species, as mentioned in Table 1, were used as input for the simulations. The experimental temperature profiles were also used as input, restricting the simulations to solve for species transport equation. The temperature imposed at HAB = 0 cm is 298 K for all the simulations. Multi-component species transport and the thermal diffusion effect (Soret effect) were considered in the calculation. The computational grid was refined to obtain gradient and curvature parameters as 0.1 and 0.4, respectively. Further reduction of these parameters led to non-convergence of the simulations.

Several chemical kinetic models are available in the literature for H_2 combustion. However, most of these models do not include NO_X sub-chemistry, see e.g. [45–47]. Those including the nitrogen chemistry [48,49] were validated against experimental data in H_2, but also in NH_3 oxidation. Indeed, the complex chemistry of intermediate species such as N_2Hx [50], or HNNO and its isomers [25,51], is indispensable. The most recent studies into the development of detailed H/O/N kinetic models have focused on NH_3 oxidation, with more than 30 detailed kinetic models in the last 2 decades. In essence, these models include both hydrogen and nitrogen sub-chemistry with recent updates of thermochemistry, and have been developed taking into account NO speciation carried out in different lab-scale reactors. In this study, the chemical kinetic models developed by Zhu et al. [52], Jian et al. [53], and Stagni et al. [54] have been used for the numerical simulation. The simulations using these models are referred to here as Zhu2024, Jian2024, and Stagni2023.

3.2. Pathway analysis

The extraction of NO formation pathways from the numerical results is challenging due to the dynamic interplay between the different pathways. In the literature, the NO formation pathway has been extracted by grouping reactions by sub-mechanisms, simulations with only the NO sub-mechanism of interest, or by removing the initiation reactions of the NO sub-mechanisms and calculating the difference to the full-chemistry solution. However, isolating a specific NO sub-mechanism and calculating its contribution to total NO formation is complex because some elementary reactions simultaneously participate in multiple NO sub-mechanisms [36].

Another possibility for interpreting the NO formation pathway is tracking the amount of NO formed by each elementary reaction involving NO. This NO pathway analysis method is inspired by the works of [55–57]. The NO concentration coming from each reaction can be calculated by Eq. 4 [56]:

$$[\mathrm{NO}(\tau)]_S = \int_0^{\tau} \omega_S(t) \times d(t) \tag{4}$$

where $[NO(\tau)]_S$ is the NO concentration formed at residence time τ by the reaction S, $\omega_S(t)$ is the rate of the reaction S as a function of t. The residence time t is calculated using the axial velocity predicted by the numerical simulation. This method is referred to here as integral flux analysis of the species. The advantage of the integral flux analysis is that the resulting concentration from the integration can be compared with the experimental mole fraction to check for the consistency of the analysis. The integral flux analysis of the species can highlight the precursors that have made substantial contributions to the formation/consumption of the species. The analysis can be iterated backward step-by-step for every precursor until the starting species, N_2. For example, the integral flux analysis of NO reveals that NNH is a necessary precursor. The analysis is repeated for NNH, which shows that N_2 is the source of NNH. Thus, the formation pathway from N_2 to NO can be traced quantitatively using this approach. The results from Zhu2024 have been used for this analysis since they show better agreement with the experiments. The integral flux analysis uses the reversible reaction rates calculated by Zhu2024. Table S1 in the Supplementary Information provides the absolute amount formed and consumed for each species in all the flame conditions. The figures discussed in Section 4.1.2 consider the reactions that contribute at least 2 % to the formation/consumption of species in any of the flames. The relative contribution of each reaction is calculated by normalizing the reaction's contribution against the total amount formed/consumed. The reaction numbers shown in the figures correspond to those used in Zhu2024.

4. Results and discussions

In this study, the NO mole fraction and temperature profiles have

been measured along the vertical axis of the burner. The error bars represent the total uncertainty in the experimental data as described in Section 2.6. All the results discussed in Section 4.1 are for flames at 35 Torr (4.667 kPa). Section 4.2 compares the results for ϕ = 1.50 flames at 35 Torr (4.67 kPa) and 70 Torr (9.33 kPa).

4.1. Effect of φ on NO formation

4.1.1. Experimental and simulation results

Fig. 5a-5e show the temperature and NO mole fraction profiles in ϕ = 0.35, 0.60, 1.05, 1.30, and 1.50, respectively, at 35 Torr. The blue circles represent the experimental NO mole fractions, and the red triangles represent the temperature obtained from the experiments. It is evident from the figures that the maximal temperature in these flames remains below 1500 K. The temperature profiles demonstrate that all the flames are close to the burner surface except for ϕ = 0.35. The experimental maximal NO mole fraction is less than 1 ppm for all the flame conditions. Fig. 5f compares the temperature and NO mole fraction as function of ϕ at HAB = 3.5 cm. The flames ϕ = 0.60 and 1.05 record the highest temperature at 1400–1450 K (including experimental uncertainty). A trend can be observed in the NO mole fractions as ϕ changes. With an increase in ϕ from 0.35 to 0.60, the NO mole fraction increases by more than 2.5 times. As ϕ increases from 0.60 to 1.05, the mole fraction increases by 20 % to 0.71 ppm, the highest mole fraction among all the flames at HAB = 3.5 cm. On further increase in ϕ, the NO mole fraction decreases steeply. The NO mole fraction decreases by 50 % (approximately) as ϕ increases from 1.05 to 1.30 and by another 50 % from 1.30 to 1.50.

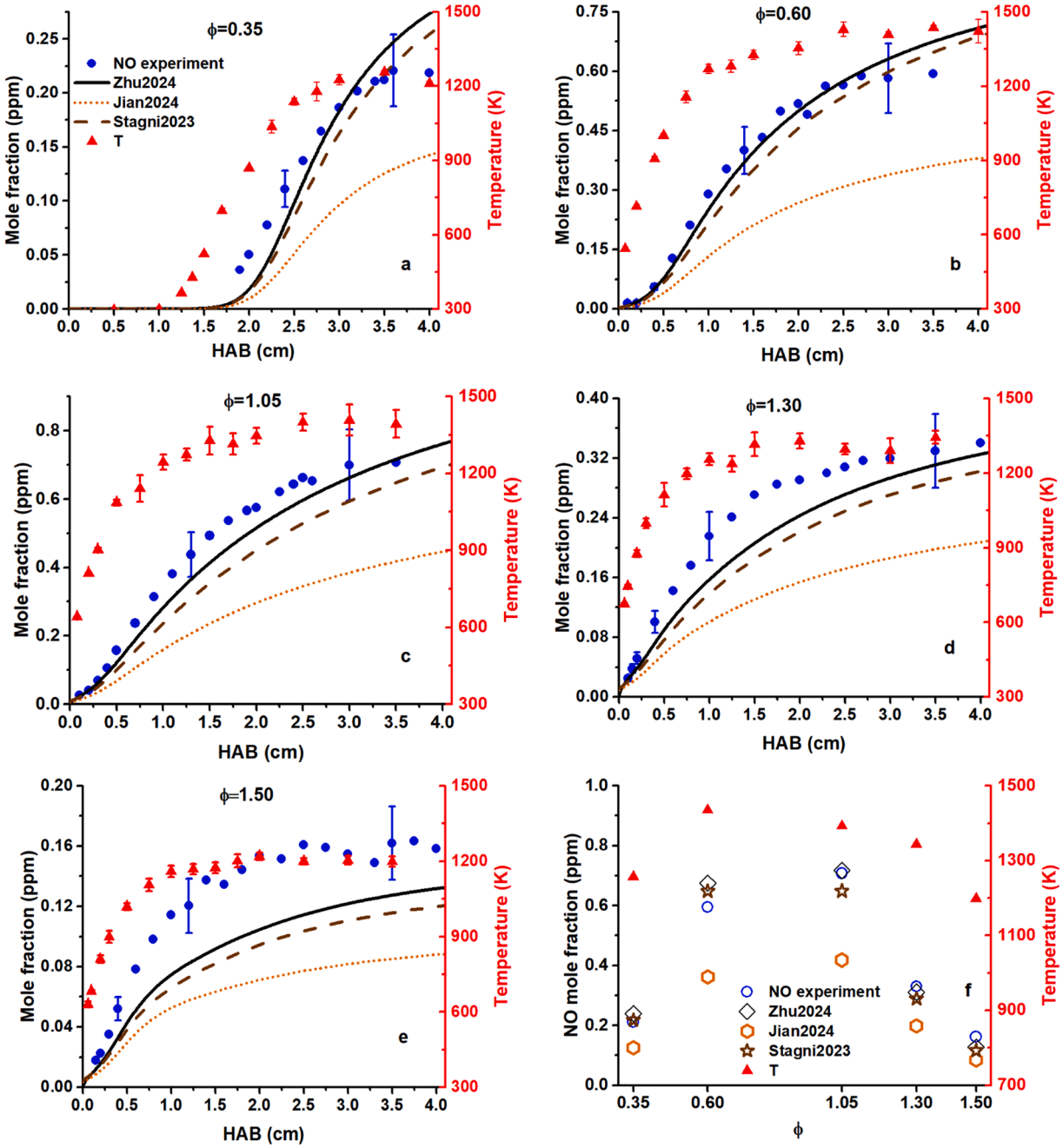

Fig. 5. Temperature (T) and NO mole fraction profiles (symbols-experimental; lines-numerical) in a. ϕ=0.35, b. ϕ=0.60, c. ϕ=1.05, d. ϕ=1.30 and e. ϕ =1.50 flames. f. Comparison of NO mole fraction and temperature (T) at HAB=3.5 cm for ϕ=0.35–1.50. Blue circle-experimental NO, grey diamond-Zhu2024, orange hexagon-Jian2024, brown star-Stagni2023, and red triangle-temperature.

Fig. 5 also shows the simulated NO mole fractions obtained using the three chemical kinetic models. Overall, the simulations can capture the trends of the experimental profiles. The predictions from Zhu2024 (solid black line) and Stagni2023 (dashed brown line) are in satisfactory agreement with the experiment for $\phi = 0.35$, 0.60, and 1.05. The predictions from these two models deviate slightly from the experimental data for both $\phi = 1.30$ and $\phi = 1.50$ flames. However, Jian2024 (dot orange line) underpredicts the NO mole fractions by 40 % for all the flames.

4.1.2. NO formation pathway analysis for flames at 35 Torr (4.667 kPa)

The satisfactory agreement between the experiments and the predictions from Zhu2024 provides an opportunity to explore the NO formation chemical pathways using detailed chemical reactions. Interestingly, Zhu2024 incorporates the HNNO subset which, according to Meng et al. [51] and Lee et al. [25], plays an important role in NOx formation. The integrated flux analysis of the species was used to identify the crucial intermediates involved in transforming N_2 to NO. The flux analysis for N_2 (please see Section S2a in Supplementary Information) reveals that more than 99 % of its consumption is involved in forming NNH, irrespective of the equivalence ratio. Hence, NNH is a crucial intermediate in all the flames studied here.

4.1.2.1. NNH flux analysis. The results of integral flux analysis of NNH are presented in Fig. 6a. Fig. 6b shows the mole fraction profiles of NNH in the flames. Fig. 6a reveals that N_2 is the sole source of NNH for all the flame conditions. Bozzelli and Dean [7] predicted that the forward and the reverse reactions of R153, NNH⇌H+N_2, are influenced by tunneling, making both reactions fast enough to maintain partial equilibrium with NNH at typical combustion conditions. The values considered for NNH lifetime and heat of formation ($\Delta_f H^0_{298}$) determine the feasibility of NNH equilibrium. The NNH lifetime, which is inversely proportional to the rate coefficient of the NNH dissociation reaction, should be small enough so that the dissociation and formation of NNH are fast [8]. In the literature, the NNH lifetime ranges from 36 ns [58] to 0.4 ns [59]. Bozzelli and Dean [7] adopted an NNH lifetime of 3 ns for the ground vibrational state and an activation energy of 7.4 kcal/mol, resulting in the NNH dissociation rate coefficient as 6×10^7 s^{-1} at 1000 K. On the contrary, Klippenstein et al. [8] considered a lifetime of 1 ns without any activation energy, resulting in an NNH dissociation rate coefficient of 1×10^9 s^{-1}, irrespective of the temperature. The NNH dissociation rate coefficient used by Jian2024 and Stagni2023 is the same as that used by Klippenstein et al. [8]. The rate coefficient adopted in Zhu2024 is 3×10^8 s^{-1}. Bozzelli and Dean [7] asserted that if the NNH dissociation rate is higher than 1×10^7 s^{-1}, the NNH concentration is controlled by thermodynamics and is independent of the rate coefficients of the reaction R153.

The NNH equilibrium concentration depends on the equilibrium constant of the reaction R153, which in turn depends on $\Delta_f H^0_{298}$ of NNH. The NO formation is sensitive to the value of $\Delta_f H^0_{298}$(NNH); if the value increases by 1.5 kcal/mol, the NO production will decrease by a factor of 2 [8,32]. Haworth et al. [60] derived $\Delta_f H^0_{298}$(NNH) as 60.6 kcal/mol. Hayhurst and Hutchinson [29] derived the ΔH of the reaction N_2+H⇌NNH at 2000 K as 5.49±1.6 kcal/mol (equivalent to $\Delta_f H^0_{298}$(NNH) = 60.3 kcal/mol calculated using thermodynamic data from Zhu2024) by fitting the kinetic equation to their experimental NO data. Konnov et al. [50] adopted a 59.8 kcal/mol value from [61]. Using a detailed calculation, Bozkaya et al. [58] predicted $\Delta_f H^0_{298}$(NNH) as 59.7 kcal/mol. This value was adopted by Klippenstein et al. [8] and Jian2024. The value used in Zhu2024 is 59.2 kcal/mol, and that in Stagni2023 is 59.6 kcal/mol.

Most of the NNH consumption leads to the recycling of N_2. The recycling reaction R155, NNH+O_2⇌HO_2+N_2, dominates under fuel-lean conditions, while reaction R158, H+NNH⇌H_2+N_2, dominates under fuel-rich and stoichiometric conditions. The forward reaction of R155 involves barrierless H abstraction from NNH to form highly exothermic HO_2 and N_2 [8,58]. The forward reaction of R158 involves the formation of highly exothermic products, H_2, and N_2 [7], which consequently favors the recycling of NNH to N_2. Fig. 6a shows that as φ increases, the contribution of R158 also increases. Hence, increasing H concentration in the flame increases NNH formation through the backward reaction of R153 but simultaneously increases N_2 recycling through R158, resulting in less NNH available for NO formation. Fig. 6b shows the calculated NNH mole fraction profiles. At constant dilution ratio from $\phi = 0.35$ to 1.3, NNH peak mole fraction increases by a factor of 3.7, then NNH slightly decreases at $\phi = 1.5$ where the dilution ratio is reduced by 19 %. It is worth noting that H_2 mole fraction in the inlet fuel follows the same trend. There is a substantial amount of NNH even in the post-flame regions, albeit decreasing with increasing HAB. The simulation results suggest that NNH is formed throughout the flame and not only in the flame front. The consumption of NNH either leads to NO and NH or N_2O formation.

4.1.2.2. N_2O flux analysis. The relative contributions of the reactions that form or consume N_2O are shown in Fig. 7a. Fig. 7b shows the rate of these reactions and the total N_2O reaction rate along HAB in the $\phi = 1.05$ flame. These reactions follow a similar trend in other flames. N_2O is primarily formed from NNH via reaction R163, NNH+O⇌H+N_2O, similarly observed in hydrogen counterflow diffusion flames [30]. The contribution of the direct recombination of N_2 and O reaction (reverse reaction of R183, N_2+O(+M)⇌N_2O(+M)) to N_2O formation is distinctively low, even under fuel-lean conditions. Durocher et al. [34] found

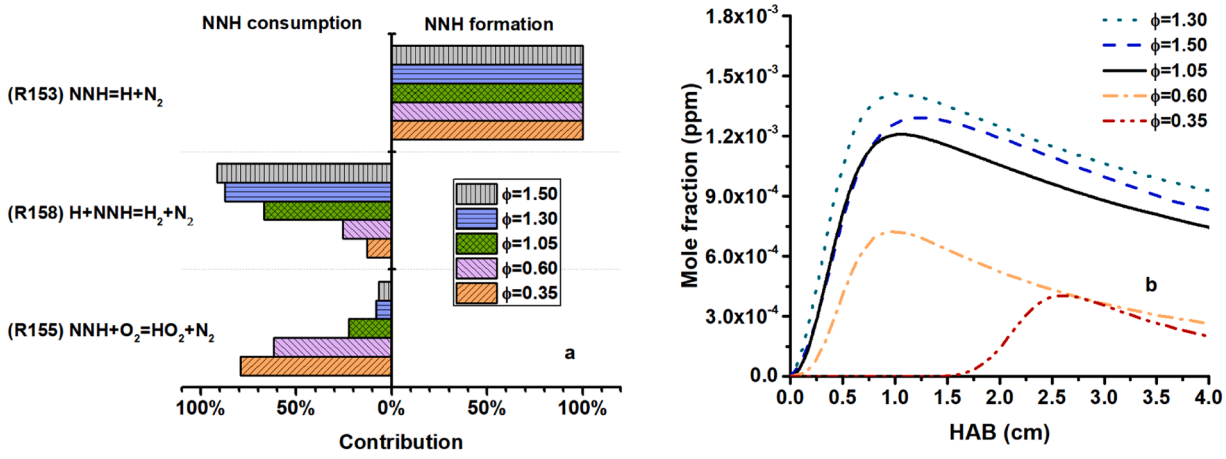

Fig. 6. Formation and consumption of NNH. a, relative contribution of the involved reactions. b, calculated NNH mole fractions profiles for ϕ =0.35–1.5 flames.

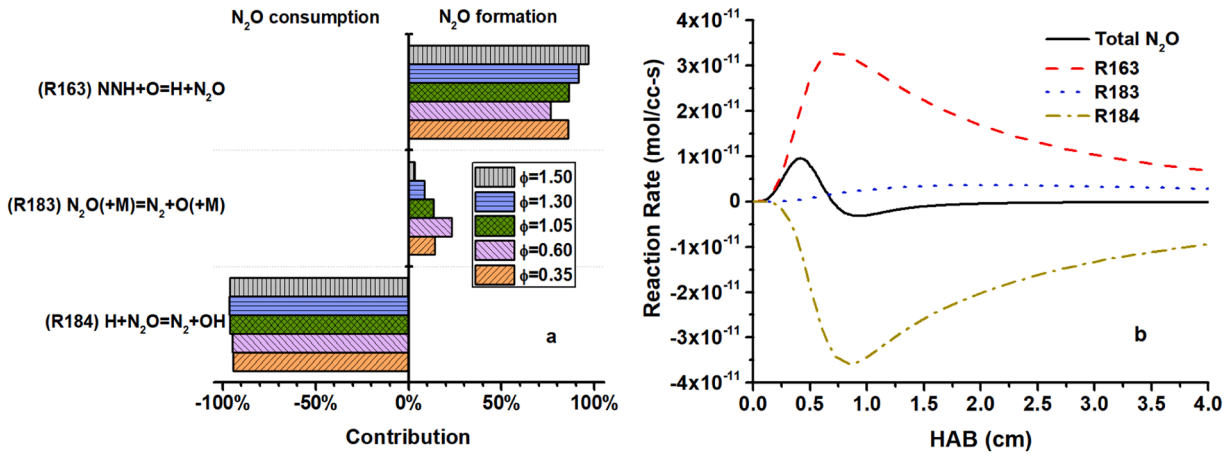

Fig. 7. Formation and consumption of N_2O. a, relative contribution of the involved reactions. b, rate of reactions that form and consume N_2O as a function of HAB in ϕ =1.05 flame.

that even at 8 atm, the contribution of reaction R183 towards N_2O formation is less than that of reaction R163. It can be anticipated that due to the pressure dependency, reaction R183 is dominant at higher pressures and/or temperatures. Fig. 7b shows that the peak of reaction R163 is early in the flame, while reaction R183 reaches a constant value later and gradually, suggesting that R163 is faster than R183.

Most of the N_2O consumption leads to N_2 recycling through reaction with H. The reaction of N_2O with H leads to two competing reactions [33]: (R184) $H+N_2O \rightleftharpoons N_2+OH$ and (reverse of R93) $NH+NO \rightleftharpoons H+N_2O$. The rate coefficients of these two reactions remain virtually unchanged for the pressure range of 0.001 to 100 atm [62]. However, reaction R184, being exothermic, is favored at low and intermediate temperatures, while the reverse reaction of R93 has a comparable contribution for temperatures above 2500 K [62]. Fig. 7b shows that the reaction R184 peaks just after reaction R163 reaches the maximum.

The small fraction (≈1 %) of NNH and N_2O that survives N_2 recycling produces NH and NO by reacting with H. Section S2b in the Supplementary Information discusses the integrated flux analysis of NH. Most of the NH comes from NNH. Under fuel-lean conditions, the consumption of NH contributes almost equally to N and NO formation. For stochiometric and rich flames, most of the NH consumption leads to the formation of N. Section S2c in the Supplementary Information shows the integrated flux analysis of N. The consumption of N in its entirety leads to NO formation in all the flames.

4.1.2.3. NO flux analysis. Fig. 8a shows the reactions that contribute substantially to the formation and consumption of NO. Fig. 8b shows the contribution of the immediate NO precursors towards NO formation. The contribution of N_2O towards NO formation is low, the maximal contribution being 4 % for $\phi = 0.60$, and it decreases to 0 for the flame $\phi = 1.50$. NH contributes substantially to NO formation under lean conditions, and its contribution decreases rapidly for equivalence ratios greater than 0.60. Unlike NH, N contributes significantly to NO formation under stoichiometric and fuel-rich conditions. Under fuel-lean conditions, the contributions from NH and N are comparable. NNH is the most significant contributor to NO formation for the flames $\phi = 0.35$ to $\phi = 1.30$. For the flame $\phi = 1.50$, NNH is the second largest contributor. NNH to NO is converted through the reaction R162, $NNH+O \rightleftharpoons NH+NO$. This reaction has the maximal contribution towards NO formation in the flame $\phi = 0.35$, and the contribution decreases slightly with an increase in ϕ. The rate coefficient of reaction R162 varies by more than one order of magnitude in the literature, causing discrepancies in the NO predictions [1]. Section S2f in the Supplementary Information discusses the different rate coefficients of R162 as found in the literature. The reaction of NNH and O leads to three competing channels: (R154) $NNH+O \rightleftharpoons N_2+OH$, (R162) $NNH+O \rightleftharpoons NH+NO$, and (R163) $NNH+O \rightleftharpoons H+N_2O$. Bozzelli and Dean [7] predicted that the NH+NO product channel (R162) is the major channel since the other two channels are restricted by entropy (for R163) and isomerization through a tight transition state (for R154). On the contrary, Haworth et al. [60] and Klippenstein et al. [8] predicted reaction R162 as the minor channel due to the endothermicity of the products NH and NO. Other than NNH, HNO also makes a substantial contribution to NO formation. Its contribution increases steadily with an increase in ϕ. In fact, for ϕ=1.50, the reaction R192, $H+HNO \rightleftharpoons H_2+NO$, has the maximal contribution towards NO formation. NO_2 also

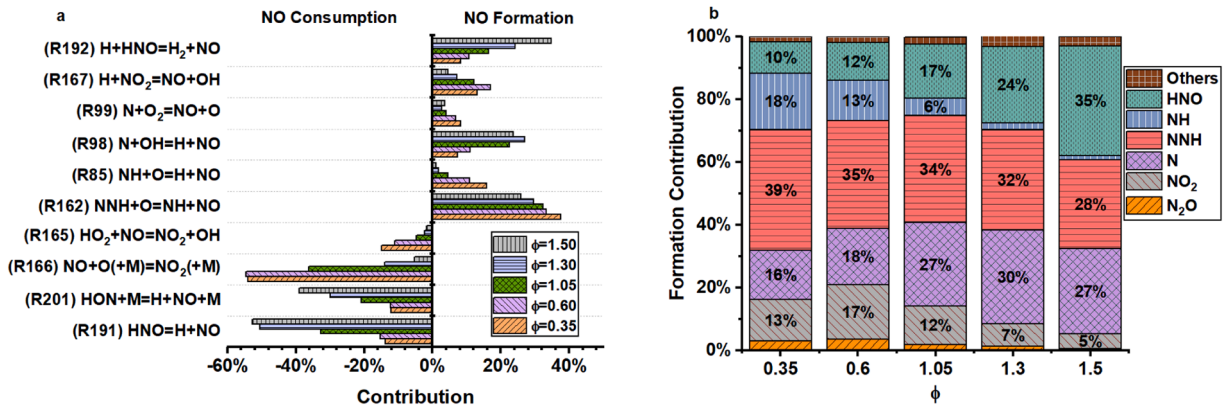

Fig. 8. Formation/consumption of NO. a, Reactions with substantial contribution. b, Contributions of NO precursors towards NO formation.

contributes towards NO formation, with relatively higher contributions for lean and stoichiometric flames. There are also minor (less than 4 %) contributions from other species (e.g., HON, HONO, NH_2, t-ONNH) towards NO formation. In Fig. 8b, the cumulative contribution of these species is referred to as others. The NO flux analysis shows two distinct channels of NO depletion. For lean and stoichiometric flames, the primary product of NO consumption is NO_2, while for rich flames, the primary product is HNO and HON.

For a comprehensive analysis of NO formation, it is essential to analyze the formation and consumption of HNO and NO_2. Detailed analyses are provided in Sections S2d and S2e in the Supplementary Information. In all the flames, HNO is formed from HON, which itself is formed through the reverse reaction of R201, HON+M⇌H+NO+M. In the lean flames, NH provides an additional contribution to HNO formation. HON also leads to the formation of NO_2 in the stoichiometric and rich flames. In the lean flames, NO_2 is formed directly from NO. The consumption of both NO_2 and HNO in entirety leads to NO formation for all the flames.

4.1.2.4. Summary of integrated flux analysis. A comparative analysis of the NO formation pathway for different equivalence ratios can be performed by tracking the consumption flux of the species, starting from N_2. Fig. 9a summarizes the pathway. The color-coded numbers above the arrows represent the percentage of the consumption of the species through that channel for different ϕ. Fig. S9 (in the Supplementary Information) represents the same scheme of the NO formation pathway but in moles.cm^{-3} unit. Fig. 9b shows the temporal distribution of the key intermediates in the ϕ = 1.05 flame. The distribution trends of these intermediates in other flames are similar.

As shown in Fig. 9a, the decomposition of N_2 mainly leads to NNH formation for all ϕ. The thermal NO formed in these flames was checked by numerical simulation to be 2 orders of magnitude less than the non-thermal NO. The percentage of N_2 consumption that leads to N_2O formation is insignificant for all the flame conditions. More than 95 % of NNH consumption leads to N_2 recycling, with this percentage increasing sharply as ϕ rises more than 1. Under stoichiometric and fuel-lean conditions, 2–3 % of NNH consumption contributes to N_2O formation. Fig. 9b shows that the calculated N_2O mole fraction peaks before NNH, suggesting that the N_2O formation from NNH commences as soon as NNH is formed. The contribution of NNH consumption towards NO and NH formation is very low (almost 1/3 of the contribution for N_2O formation), decreasing with increasing ϕ. Most N_2O consumption leads to N_2 recycling. A similar trend has been observed in atmospheric lean premixed jet-wall stagnation H_2/air flame [33]. It is worth noting that the channels involving N_2O leading to the direct formation of NO, (reverse of R93) NH+NO⇌H+N_2O and (R186) N_2O+O⇌2NO, are significant only at temperatures higher than 2500 K and 1850 K, respectively [6,62]. The flames studied here show that there is considerable N_2 recycling through the channel N_2→NNH→N_2, while Durocher et al. [34] found that the recycling involves the channel N_2→NNH→N_2O→N_2. The percentage of N_2O consumption for NO formation is higher than that for NH formation under fuel-lean conditions. In contrast, the contribution is equal for the two channels under stoichiometric and fuel-rich conditions. Most of the NH consumption in the lean flames leads to NO and N formation, but under stoichiometric and fuel-rich conditions, most of the NH consumption leads to N formation. NH and N mole fractions peak just after N_2O but before NNH peaks (Fig. 9b). A small amount of NH consumption also forms HNO under fuel-lean and stoichiometric conditions. The consumption of N and HNO in their entirety produces NO. There are two NO recycling channels. Under fuel-lean conditions, the recycling channel involves NO→NO_2→NO. The recycling channel dominant in the rich flames involves NO→HNO→NO. For the stoichiometric flame, both these recycling channels are equally dominant. The analysis shows that the NNH pathway is dominant for all ϕ. Recent studies show that the NNH pathway is the primary pathway of NO formation in premixed hydrogen flames at atmospheric and higher pressures [33,34]. The N_2O pathway does not have any substantial contribution to NO formation for any ϕ. Conversely, the hydrogen combustion study in an atmospheric pressure jet-stirred reactor shows that the N_2O pathway is dominant under lean conditions [31].

4.2. Effect of pressure on NO formation in ϕ=1.50 flames

As mentioned earlier, the combustion community relies heavily on experimental NO measurements to validate the NNH sub-mechanism due to the unavailability of the experimental rate coefficient. Thus, the experimental NO measurements performed by Harrington et al. [32] in H_2/air premixed flames with ϕ = 1.50 at 38 Torr (5.1 kPa) and 78 Torr (10.4 kPa) are crucial for validating NNH chemical models. As specified by the authors [32], the low temperature of the flames mitigates thermal NO formation, while the low pressure and fuel-rich condition suppresses the N_2O formation directly from N_2. The fuel-rich condition also ensures adequate H concentration for NNH formation. Thus, the experimental conditions favor NO formation from NNH but suppress the other pathways [32]. Several numerical studies have been performed to predict the NO mole fractions of these flames. The numerical studies in [8,60,63]

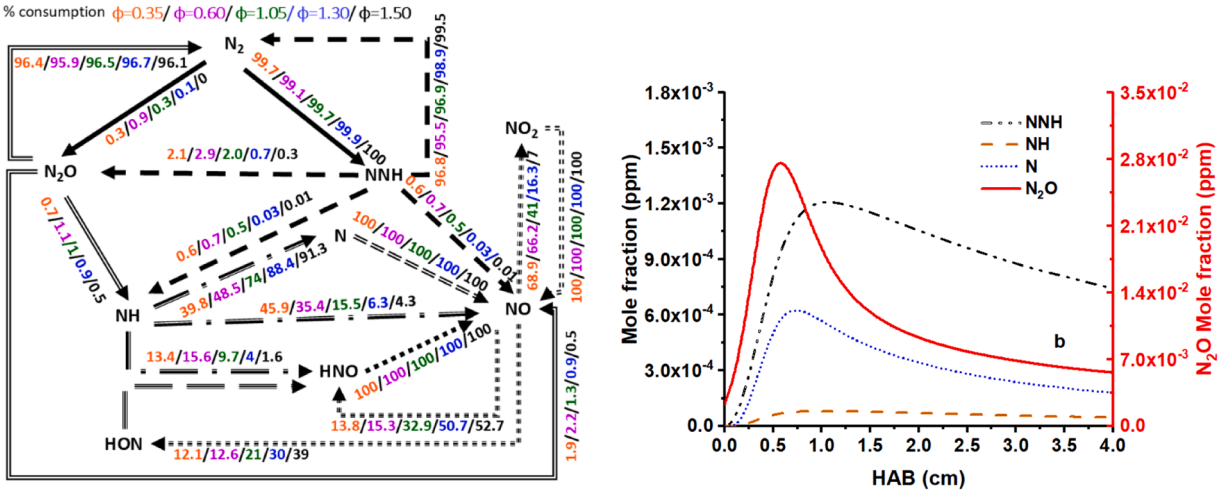

Fig. 9. Analysis of the NO formation pathway. a, Simplified schematic of NO formation pathway. The numbers above the edges represent the percentage of the precursor consumed. Colors: Orange: ϕ=0.35, Magenta: ϕ=0.60, Green: ϕ=1.05, Blue: ϕ=1.30, Black: ϕ=1.50. b, Calculated mole fractions of intermediates in ϕ=1.05 flame.

cannot predict any of the flame conditions while the numerical studies in [5,32,48] can only predict the 78 Torr flame conditions. Klippenstein et al. [8] and Glarborg et al. [1] remarked that since the comparison between the experiments and simulation predictions is inconclusive, novel NO measurements are necessary for validating the NNH mechanism.

Harrington et al. [32] stabilized 2 flames above a McKenna burner as in the current study, with a pressure ratio close to 2. However, some experimental parameters are not specified in their paper: the material and the cooling temperature of the central porous, the pressure and temperature at which the total flow rate of 6 l/min was measured. In the current study, quantitative NO measurements have been performed in flames slightly differing from Harrington's (different total flow rate and slightly different pressures) to guarantee flame stability, while maintaining the same fuel mixture composition as for Harrington. The total volumetric flow rate in the current study is 4.65 slpm. In addition to the ϕ =1.50 flame already described at p = 35 Torr, a supplementary flame (same ϕ and total volumetric flow rate) stabilized at 70 Torr (9.33 kPa) was studied for a comprehensive comparison with Harrington's data. The impact of the change of the flame conditions between the current study and those in [32] on NO formation will be discussed below.

It is worth noting that adopting the flame conditions similar to that of Harrington et al. results in a low amount of NO, which imposes significant challenges on recording LIF signals. A meticulous experimental approach and careful consideration of potential sources of error and uncertainty were necessary to quantify NO under these flame conditions (see Supplementary Information S1 and section 2.3). Fig. 10a and 10b show the temperature and NO mole fractions measured in this study at 35 Torr and 70 Torr, respectively. Fig. 10c and 10d show the temperature and NO mole fractions at 38 Torr and 78 Torr, respectively, as reported by Harrington et al. [32]. The temperature profiles measured in the two flames of the current study are similar to the ones recorded by Harrington et al. The peak temperature is 1200 K for all the flames. The peak NO mole fraction in the 35 Torr flame of the current study is 0.16 ppm, almost half of what was measured by Harrington et al. at 38 Torr ($\approx$ 0.3 ppm). On increasing the pressure from 35 Torr to 70 Torr, the peak NO mole fraction decreases to 0.09 ppm. On the contrary, the measurements of Harrington show that the peak NO mole fraction increases from 0.3 ppm to 0.4 ppm as pressure increases from 38 Torr to 78 Torr.

All the flames have been simulated using the three chemical kinetic models. Of course, the predicted NO mole fractions in the burned gases depend on the selected flame conditions. As shown in Fig. 10, the predictions from Zhu2024 and Stagni2023 agree satisfactorily with the experimental mole fraction measured in the 35 and 70 Torr flames (current study). Jian2024 underpredicts these flames by a almost a factor of 0.5. On the contrary, all the chemical models underpredict the NO mole fractions for the Harrington flame conditions. The numerical predictions show that the NO mole fraction decreases with increasing pressure, both for the current study and for Harrington conditions. This means that the above-mentioned trend is not affected by the difference in total flow rate and the slight difference in pressure between our study and that of Harrington et al. [32]. To better assess the impact of increasing pressure on the NO mole fraction, the measured and simulated mole fraction ratios are shown in Fig. 11. Indeed, the absolute quantification procedure of LIF signals has its inherent uncertainties, which might affect the interpretation of the effect of pressure increase on the mole fraction. The LIF signals in the ϕ = 1.50 flames at 35 and 70 Torr were compared directly to avoid these uncertainties. To this end, the LIF signals in the two flames at 35 Torr and 70 Torr were measured at

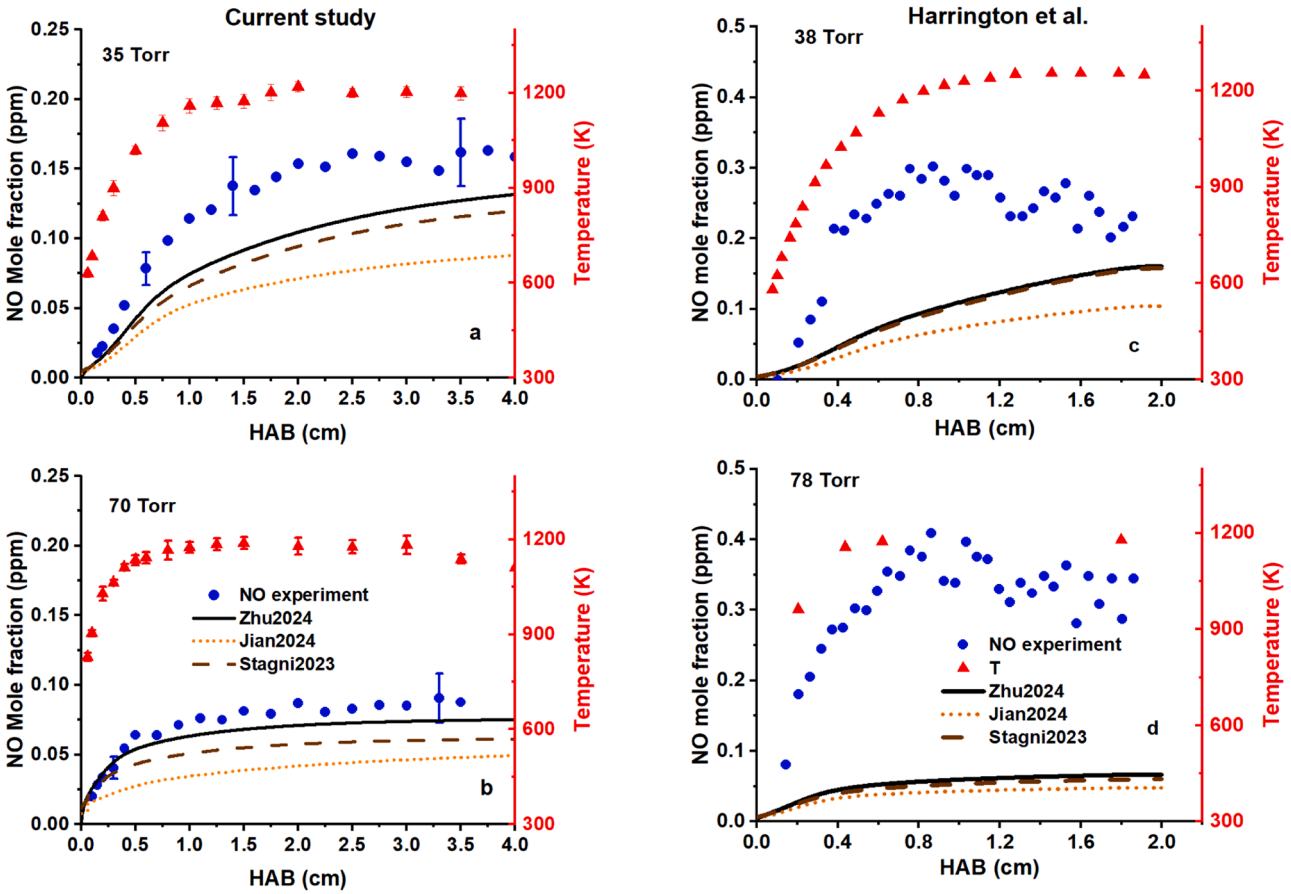

Fig. 10. Temperature (T) and NO mole fractions in flame ϕ=1.5 at a) 35 Torr and b) 70 Torr recorded in the current study (left side), at c) 38 Torr and d) 78 Torr, as measured in [32] (right side).

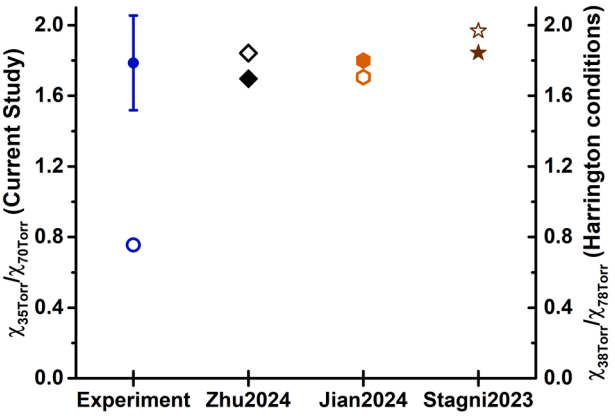

Fig. 11. Ratio of NO mole fraction in the flames ϕ=1.50 at 35 Torr and 70 Torr at HAB = 3.0 cm, and 38 Torr and 78 Torr at HAB = 1.0 cm. Filled symbols: Current study (left y-axis), empty symbols: Harrington flame conditions (right y-axis).

HAB = 3.0 cm because all flame switch and calibration procedures were performed at this height, ensuring higher confidence in these measurements (Fig. S10 of the Supplementary Information). For the reader's convenience, the LIF ratio has been treated considering the pressure ratio to derive the mole fraction ratio. Fig. 11 (left Y-axis) shows that the experimental NO mole fraction (filled blue circle) in 35 Torr flame is 1.82 times more than 70 Torr flame at HAB = 3.0 cm. The NO mole fraction ratios predicted by the models (filled symbols) for the flames at 35 and 70 Torr closely agree with the experimental values. This satisfactory agreement between the experiment and numerical values suggests that the models can capture the decrease in NO mole fraction as pressure increases from 35 Torr to 70 Torr. In Harrington's flames, this trend was evaluated at HAB = 1 cm where the LIF signal is maximum ensuring the best signal/noise ratio (Fig. 11, right Y-axis). The ratio of mole fractions (empty blue circle) at 38 Torr and 78 Torr, according to Harrington et al. [32] is 0.76, while the simulations show that the ratio for these flame conditions is in the range of 1.7 to 1.96. The decrease in simulated NO mole fraction by a factor of 1.8 with doubling of pressure is observed regardless the flame condition and model. Fig. S11 in the Supplementary Information shows that the NO concentration in the two flames remains almost the same. Hence, from increasing the pressure from 35 Torr to 70 Torr, there is no significant change in the NO sub-chemistry in the two flames. Consequently, the current set of NO mole fraction measurements in the two ϕ= 1.50 flames accurately accounts for the pressure effect, providing a robust validation dataset for the NNH pathway.

The reason for the discrepancy between the two sets of measurements is not apparent. Harrington's experiments were performed almost 30 years ago with an acquisition system that is less accurate than the ones used nowadays. Notably, the LIF signals recorded by Harrington et al. were temporally integrated over 15 ns using a boxcar integrator. Although quenching corrections are necessary for such temporal integration, the authors did not perform such corrections. In the current study, it has been verified in two steps that the prompt-LIF (temporal peak of the LIF signals) does not need to be corrected for quenching variation. First the mole fraction at 70 Torr (ϕ = 1.5) was determined from the LIF switch (L.S.) with two flames at 35 Torr (ϕ = 1.05 and ϕ = 0.35), in which the native NO was determined by the standard addition method (section 2.5). This procedure led to a value of 0.08 ppm at HAB = 3.0 cm in the 70 Torr flame for both the L.S. Second, the standard addition method was applied separately at 70 Torr flame to calibrate the NO LIF signal at the same HAB, which yielded a value of 0.07 ppm. The difference between the two values is within the limits of experimental uncertainty. It is worth noting that Harrington et al. calibrated the LIF signals by doping the flame with 150 ppm of NO, more than two orders of magnitude higher than that generated in the flame whereas the calibration in the current study ranged from 0 to 8 ppm of NO. The significant difference between the calibrated value and the actual NO mole fraction formed in the flame impacts the accuracy of the native NO determination.

The comparison of the integrated NO flux analysis in the two flames can reveal the change in flame chemistry with the increase in pressure. Fig. 12 compares the reactions that substantially contribute to the formation and consumption of NO at 35 Torr and 70 Torr. There is no significant change in the relative contribution of the reactions in the two flames.

5. Conclusion

Quantitative NO measurements were performed in low-pressure burner stabilized $H_2/O_2/N_2$ flames with ϕ ranging from 0.35 to 1.50 using LIF technique. The measured temperatures (multi-line NO-LIF) show that the peak temperature in the flames remains below 1500 K. The peak NO mole fraction in all the flames remains below 1 ppm. The highest NO mole fraction is observed in ϕ = 1.05 flame and decreases at both leaner and richer conditions. The detailed integrated flux analyses show that in all the investigated flame conditions, NO is primarily formed through NNH pathway. The contribution of N_2O pathway is insignificant while the thermal NO pathway is negligible. As ϕ changes, the relative contribution of the reactions changes, but the overall NO formation pathway virtually remains the same.

The new set of NO measurements in the flames, similar to Harrington et al. [32], accounts for the pressure effect correctly and has been checked for consistency. Contrary to Harrington, the new set of measurements reveals that the NO mole fraction decreases as pressure increases from 35 to 70 Torr. The trends observed in the new dataset are consistent with the simulation predictions performed in the literature. Since the Harrington dataset has been the only reference dataset for the NNH pathway for three decades, the significant disagreement between the Harrington experimental dataset and the numerical predictions questioned the understanding of the NNH pathway. The new NO experimental dataset in ϕ = 1.50 flame at 35 and 70 Torr can serve as potential validation targets for NNH pathway.

The comprehensive NO dataset generated in this study using rigorous experimental protocol helped assess the current understanding of the NO formation pathways in hydrogen flames. Zhu2024 and Stagni2023 can satisfactorily predict the NO mole fraction in all the flame conditions. Due to the reliability of the experimental dataset and the satisfactory agreement between the simulation predictions and the experimental data, a detailed NO formation pathway analysis was possible. The analysis indicates that the NNH pathway is the dominant pathway of NO formation under all flame conditions. The contribution of thermal NO pathway is negligible. The contribution of N_2O to NO

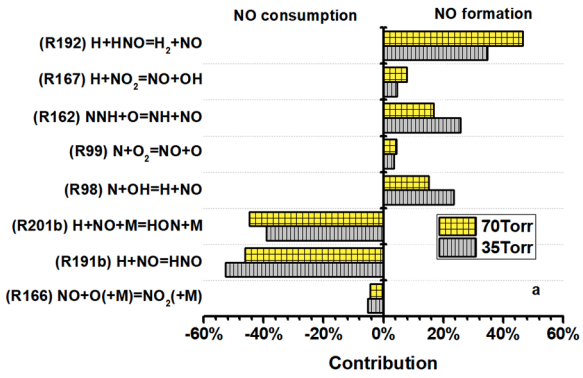

Fig. 12. Comparison of the contribution of the reactions with substantial contribution to the formation and consumption of NO in flames ϕ=1.50 at 35 Torr and 70 Torr.

formation is insignificant. The overall pathway of NO formation does not change with ϕ. Only the relative contributions of the intermediates change as ϕ changes. The NNH formation continues throughout the flame and not only in the flame front. However, the NO formation is intrinsically linked to the concentrations of non-nitrogen-containing radicals like O, OH, and H [35]. In this study, it has been assumed that the chemical kinetic models can predict the radical pool concentration accurately. Future studies should focus on assessing the accuracy of the hydrogen base chemistry and its effect on NO formation.

Novelty and significance statement

This study addresses a critical knowledge gap in non-thermal pathways (NNH and N_2O) of NO formation during H_2 combustion. More specifically, the only experimental dataset by Harrington (Harrington et al., Symp. (Int) Combust. 26 (1996)), that has been used for the last 3 decades to validate the NNH pathway, showed significant discrepancies with the simulation predictions and led to a perception that our current NO formation understanding is incomplete. The re-evaluated dataset for Harrington flame conditions resolves the existing discrepancy. The rigorous experimental protocol applied here allowed the quantification of very low amount of NO (0.15–1 ppm in the burnt gases) formed in the flames over wide range of equivalence ratio (0.35–1.5). Thanks to the robust experimental dataset, we now know that two recent chemical kinetic models can capture the NO formation in H_2 flames satisfactorily. The dataset generated is essential for validation of future chemical kinetic models, especially for NNH pathway.

CRediT authorship contribution statement

Tirthankar Mitra: Writing – original draft, Visualization, Validation, Methodology, Investigation, Formal analysis, Data curation, Conceptualization. **Nathalie Lamoureux:** Writing – review & editing, Validation, Supervision, Project administration, Methodology, Conceptualization. **Pascale Desgroux:** Writing – review & editing, Validation, Supervision, Project administration, Funding acquisition, Conceptualization.

Declaration of competing interest

The authors declare that they have no known competing financial interests or personal relationships that could have appeared to influence the work reported in this paper.

Acknowledgments

This work was supported by a government grant managed by the Agence Nationale de la Recherche under the France 2030 program, reference ANR 22-PEHY-0014, MéOL plateforme of Univ. Lille, and by the CPER ECRIN funded by French Ministère de l'Enseignement Supérieur et de la Recherche, Regional Council "Hauts-de-France" and "European Regional Development Fund". The authors would also like to acknowledge Pascal Demaux for his electronic support.

Supplementary materials

Supplementary material associated with this article can be found, in the online version, at doi:10.1016/j.combustflame.2025.114192.

References

[1] P. Glarborg, J.A. Miller, B. Ruscic, S.J. Klippenstein, Modeling nitrogen chemistry in combustion, Prog. Energy Combust. Sci. 67 (2018) 31–68.
[2] Y. Zeldovich, D. Frank-Kamenetskii, P. Sadovnikov, Oxidation of nitrogen in combustion, Publishing House of the Acad of Sciences of USSR (1947).
[3] P.C. Malte, D.T. Pratt, The role of energy releasing kinetics in NO_x formation: fuel lean, jet stirred CO air combustion, Combust. Sci. Technol. 9 (1974) 221–231.
[4] P.C. Malte, D.T. Pratt, Measurement of atomic oxygen and nitrogen oxides in jet-stirred combustion, Symp. (Int) Combust. 15 (1975) 1061–1070.
[5] M. Skottene, K.E. Rian, A study of NO_x formation in hydrogen flames, Int. J. Hydrogen Energy 32 (2007) 3572–3585.
[6] N.E. Meagher, W.R. Anderson, Kinetics of the $O(^3P) + N_2O$ Reaction. 2. Interpretation and Recommended Rate Coefficients, J. Phys. Chem. A 104 (2000) 6013–6031.
[7] J.W. Bozzelli, A.M. Dean, O + NNH: A possible new route for NOx formation in flames, Int. J. Chem. Kinet. 27 (1995) 1097–1109.
[8] S.J. Klippenstein, L.B. Harding, P. Glarborg, J.A. Miller, The role of NNH in NO formation and control, Combust. Flame 158 (2011) 774–789.
[9] P. Glarborg, P.G. Kristensen, K. Dam-Johansen, M.U. Alzueta, A. Millera, R. Bilbao, Nitric Oxide Reduction by Non-hydrocarbon Fuels. Implications for Reburning with Gasification Gases, Energy Fuels 14 (2000) 828–838.
[10] A.A. Konnov, G. Colson, J.D. Ruyck, NO formation rates for hydrogen combustion in stirred reactors, Fuel 80 (2001) 49–65.
[11] R.J. Mainiero, M. Vanpee, Reaction Mechanisms in Hydrogen-Nitric Oxide Flames, Combust. Sci. Technol. 22 (1980) 171–183.
[12] D.J. Seery, M.F. Zabielski, Molecular beam sampling-mass spectrometer study of H_2-O_2-NO flames, Symp (Int) Combust 18 (1981) 397–404.
[13] R.J. Roby, C.T. Bowman, Formation of N_2O in laminar, premixed, fuel-rich flames, Combust. Flame 70 (1987) 119–123.
[14] R.J. Cattolica, J.A. Cavolowsky, T.G. Mataga, Laser-fluorescence measurements of nitric oxide in low-pressure $H_2/O_2/NO$ flames, Symp. (Int) Combust. 22 (1989) 1165–1173.
[15] R.J. Martin, N.J. Brown, Nitrous oxide formation and destruction in lean, premixed combustion, Combust. Flame 80 (1990) 238–255.
[16] J. Bian, J. Vandooren, P.J.V. Tiggelen, Experimental study of the formation of nitrous and nitric oxides in H_2-O_2-Ar flames seeded with NO and/or NH_3, Symp. (Int) Combust. 23 (1991) 379–386.
[17] J. Vandooren, Comparison of the Experimental Structure of an Ammonia Seeded Rich-Hydrogen-Oxygen-Argon Flame with the Calculated Ones Along Several Reaction Mechanisms, Combust. Sci. Technol. 84 (1992) 335–344.
[18] R.C. Sausa, G. Singh, G.W. Lemire, W.R. Anderson, Molecular beam mass spectrometric and modeling studies of neat and NH_3-doped low-pressure $H_2/N_2O/Ar$ flames: Formation and consumption of NO, Symp. (Int) Combust. 26 (1996) 1043–1052.
[19] D.T. Venizelos, R.C. Sausa, Laser-induced fluorescence, mass spectrometric, and modeling studies of neat and NH_3-doped $H_2/N_2O/Ar$ flames, Combust. Flame 115 (1998) 313–326.
[20] M.T. Allen, R.A. Yetter, F.L. Dryer, Hydrogen/nitrous oxide kinetics—Implications of the NxHy species, Combust. Flame 112 (1998) 302–311.
[21] M.A. Mueller, R.A. Yetter, F.L. Dryer, Flow reactor studies and kinetic modeling of the $H_2/O_2/NO_X$ and $CO/H_2O/O_2/NO_X$ reactions, Int. J. Chem. Kinet. 31 (1999) 705–724.
[22] A.V. Sepman, V.M. van Essen, A.V. Mokhov, H.B. Levinsky, Cavity ring-down measurements of seeded NO in premixed atmospheric-pressure H_2/air and CH_4/air flames, Appl. Phys. B 77 (2003) 109–117.
[23] G. Dayma, P. Dagaut, Effects of Air contamination on the combustion of hydrogen-Effect of NO and NO_2 addition on hydrogen ignition and oxidation kinetics, Combust. Sci. Technol. 178 (2006) 1999–2024.
[24] A.G. Shmakov, O.P. Korobeinichev, I.V. Rybitskaya, A.A. Chernov, D.A. Knyazkov, T.A. Bolshova, A.A. Konnov, Formation and consumption of NO in $H_2+O_2+N_2$ flames doped with NO or NH_3 at atmospheric pressure, Combust. Flame 157 (2010) 556–565.
[25] J. Lee, M.C. Barbet, Q. Meng, R.E. Cornell, M.P. Burke, Experimental support for a new NOx formation route via an HNNO intermediate, Combust. Flame 257 (2023) 112632.
[26] P. Glarborg, E. Fabricius-Bjerre, T.K. Joensen, H. Hashemi, S.J. Klippenstein, An experimental, theoretical and kinetic modeling study of the N2O-H2 system: Implications for N2O + H, Combust. Flame 271 (2025) 113810.
[27] J.B. Homer, M.M. Sutton, Nitric oxide formation and radical overshoot in premixed hydrogen flames, Combust. Flame 20 (1973) 71–76.
[28] L. Xie, S. Hayashi, K. Hirose, NOx formation in turbulent lean-premixed combustion with minimum heat losses, Symp. (Int) Combust. 26 (1996) 2155–2160.
[29] A.N. Hayhurst, E.M. Hutchinson, Evidence for a New Way of Producing NO via NNH in Fuel-Rich Flames at Atmospheric Pressure, Combust. Flame 114 (1998) 274–279.
[30] G.J. Rørtveit, J.E. Hustad, S.C. Li, F.A. Williams, Effects of diluents on NOx formation in hydrogen counterflow flames, Combust. Flame 130 (2002) 48–61.
[31] A.L. Purohit, A. Nalbandyan, P.C. Malte, I.V. Novosselov, NNH mechanism in low-NOx hydrogen combustion: Experimental and numerical analysis of formation pathways, Fuel 292 (2021) 120186.
[32] J.E. Harrington, G.P. Smith, P.A. Berg, A.R. Noble, J.B. Jeffries, D.R. Crosley, Evidence for a new no production mechanism in flames, Symp. (Int) Combust. 26 (1996) 2133–2138.
[33] A. Durocher, M. Meulemans, P. Versailles, G. Bourque, J.M. Bergthorson, Back to basics – NO concentration measurements in atmospheric lean-to-rich, low-temperature, premixed hydrogen–air flames diluted with argon, Proc. Combust. Inst. 38 (2021) 2093–2100.
[34] A. Durocher, M. Meulemans, G. Bourque, J.M. Bergthorson, Nitric oxide concentration measurements in low-temperature, premixed hydrogen-air stagnation flames at elevated pressures, Proc. Combust. Inst. 39 (2023) 541–550.

[35] M. Meulemans, A. Durocher, G. Bourque, J.M. Bergthorson, NO measurements in high temperature hydrogen flames: The crucial role of the hydrogen oxidation chemistry for accurate NO predictions, Combust. Flame 261 (2024) 113279.
[36] H. Helbig, M.D. Bohon, A novel method for quantifying variations in NO formation pathways using a sub-mechanism accounting and reaction tracing algorithm, Combust. Flame 262 (2024) 113330.
[37] R.S. Barlow, C.D. Carter, Relationships among nitric oxide, temperature, and mixture fraction in hydrogen jet flames, Combust. Flame 104 (1996) 288–299.
[38] M.S. Day, J.B. Bell, X. Gao, P. Glarborg, Numerical simulation of nitrogen oxide formation in lean premixed turbulent H2/O2/N2 flames, Proc. Combust. Inst. 33 (2011) 1591–1599.
[39] K.K. Foo, N. Lamoureux, A. Cessou, C. Lacour, P. Desgroux, The accuracy and precision of multi-line NO-LIF thermometry in a wide range of pressures and temperatures, J. Quant. Spectrosc. Radiat. Transfer 255 (2020) 107257.
[40] N. El Baba, P. Desgroux, N. Lamoureux, On the difficulty of interpreting NO-LIF measurements around 226 nm in confined ammonia flames, Combust. Flame 264 (2024) 113424.
[41] K.K. Foo, N. Lamoureux, P. Desgroux, Software Thermo NO-LIF, (2020). pc2a.univ-lille.fr/thermo-no-lif.
[42] D.D. Thomsen, F.F. Kuligowski, N.M. Laurendeau, Background corrections for laser-induced-fluorescence measurements of nitric oxide in lean, high-pressure, premixed methane flames, Appl. Opt. 36 (1997) 3244–3252. AO.
[43] N. Lamoureux, A. El-Bakali, L. Gasnot, J.F. Pauwels, P. Desgroux, Prompt-NO formation in methane/oxygen/nitrogen flames seeded with oxygenated volatile organic compounds: Methyl ethyl ketone or ethyl acetate, Combust. Flame 153 (2008) 186–201.
[44] ANSYS Chemkin R1 Inc, (2021).
[45] A. Kéromnès, W.K. Metcalfe, K.A. Heufer, N. Donohoe, A.K. Das, C.J. Sung, J. Herzler, C. Naumann, P. Griebel, O. Mathieu, M.C. Krejci, E.L. Petersen, W. J. Pitz, H.J. Curran, An experimental and detailed chemical kinetic modeling study of hydrogen and syngas mixture oxidation at elevated pressures, Combust. Flame 160 (2013) 995–1011.
[46] A.A. Konnov, Yet another kinetic mechanism for hydrogen combustion, Combust. Flame 203 (2019) 14–22.
[47] Y. Zhang, J. Fu, M. Xie, J. Liu, Improvement of H2/O2 chemical kinetic mechanism for high pressure combustion, Int. J. Hydrogen Energy 46 (2021) 5799–5811.
[48] A. Frassoldati, T. Faravelli, E. Ranzi, A wide range modeling study of NOx formation and nitrogen chemistry in hydrogen combustion, Int. J. Hydrogen Energy 31 (2006) 2310–2328.
[49] Y. Zhang, O. Mathieu, E.L. Petersen, G. Bourque, H.J. Curran, Assessing the predictions of a NOx kinetic mechanism on recent hydrogen and syngas experimental data, Combust. Flame 182 (2017) 122–141.
[50] A.A. Konnov, J.D. Ruyck, Temperature-dependent rate constant for the reaction NNH + O → NH + NO, Combust. Flame 125 (2001) 1258–1264.
[51] Q. Meng, L. Lei, J. Lee, M.P. Burke, On the role of HNNO in NOx formation, Proc. Combust. Inst. 39 (2023) 551–560.
[52] Y. Zhu, H.J. Curran, S. Girhe, Y. Murakami, H. Pitsch, K. Senecal, L. Yang, C. W. Zhou, The combustion chemistry of ammonia and ammonia/hydrogen mixtures: A comprehensive chemical kinetic modeling study, Combust. Flame 260 (2024) 113239.
[53] J. Jian, H. Hashemi, H. Wu, P. Glarborg, A.W. Jasper, S.J. Klippenstein, An experimental, theoretical, and kinetic modeling study of post-flame oxidation of ammonia, Combust. Flame 261 (2024) 113325.
[54] A. Stagni, S. Arunthanayothin, M. Dehue, O. Herbinet, F. Battin-Leclerc, P. Bréquigny, C. Mounaïm-Rousselle, T. Faravelli, Low- and intermediate-temperature ammonia/hydrogen oxidation in a flow reactor: Experiments and a wide-range kinetic modeling, Chem. Eng. J. 471 (2023) 144577.
[55] J. Luque, G.P. Smith, D.R. Crosley, Quantitative CH determinations in low-pressure flames, Symp. (Int) Combust. 26 (1996) 959–966.
[56] T.J. Held, F.L. Dryer, A comprehensive mechanism for methanol oxidation, Int. J. Chem. Kinet. 30 (1998) 805–830.
[57] A.V. Sepman, V.M. van Essen, A.V. Mokhov, H.B. Levinsky, The effects of hydrogen addition on Fenimore NO formation in low-pressure, fuel-rich-premixed, burner-stabilized $CH_4/O_2/N_2$ flames, Int. J. Hydrogen Energy 33 (2008) 5850–5857.
[58] U. Bozkaya, J.M. Turney, Y. Yamaguchi, H.F. Schaefer, The barrier height, unimolecular rate constant, and lifetime for the dissociation of HN_2, J. Chem. Phys. 132 (2010) 064308.
[59] P.J.S.B. Caridade, S.P.J. Rodrigues, F. Sousa, A.J.C. Varandas, Unimolecular and Bimolecular Calculations for HN_2, J. Phys. Chem. A 109 (2005) 2356–2363.
[60] N.L. Haworth, J.C. Mackie, G.B. Bacskay, An Ab Initio Quantum Chemical and Kinetic Study of the NNH + O Reaction Potential Energy Surface: How Important Is This Route to NO in Combustion? J. Phys. Chem. A 107 (2003) 6792–6803.
[61] A. Burcat, W.C. Gardiner, Ideal Gas Thermochemical Data for Combustion and Air Pollution Use, Ed., in: W.C. Gardiner (Ed.), Gas-Phase Combustion Chemistry, Springer, New York, NY, 2000, pp. 489–538.
[62] J.W. Bozzelli, A.Y. Chang, A.M. Dean, Analysis of the reactions $H+N_2O$ and NH+ NO: Pathways and rate constants over a wide range of temperature and pressure, Symp. (Int) Combust. 25 (1994) 965–974.
[63] N. Lamoureux, H. El Merhubi, L. Pillier, S. de Persis, P. Desgroux, Modeling of NO formation in low pressure premixed flames, Combust. Flame 163 (2016) 557–575.